ACS APPLIED MATERIALS & INTERFACES

Research Article

www.acsami.org

Polystyrene/MWCNT/Graphite Nanoplate Nanocomposites: Efficient Electromagnetic Interference Shielding Material through Graphite Nanoplate–MWCNT–Graphite Nanoplate Networking

Sandip Maiti, Nilesh K. Shrivastava, Supratim Suin, and B. B. Khatua*

Materials Science Centre, Indian Institute of Technology, Kharagpur-721302, India

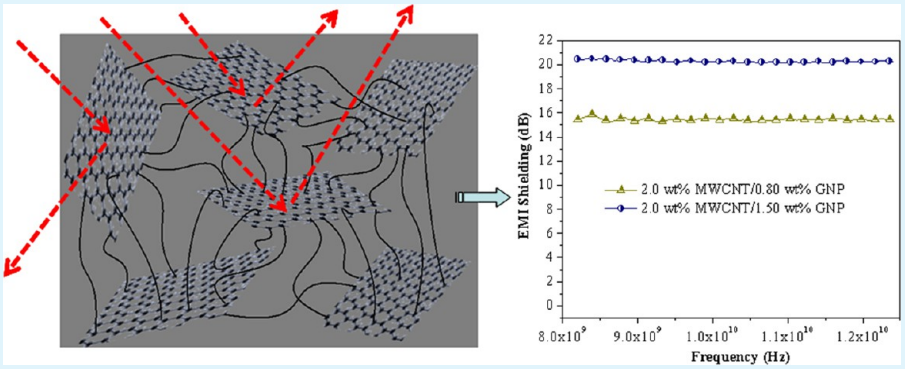

ABSTRACT: Today, we stand at the edge of exploring carbon nanotube (CNT) and graphene based polymer nanocomposites as next generation multifunctional materials. However, irrespective of the methods of composite preparation, development of electrical conductivity with high electromagnetic interference (EMI) value at very low loading of CNT and (or) graphene is limited due to poor dispersion of these nanofillers in polymer matrix. Here, we demonstrate a novel technique that involves in-situ polymerization of styrene/multiwalled carbon nanotubes (MWCNTs) in the presence of suspension polymerized polystyrene (PS)/graphite nanoplate (GNP) microbeads, for the preparation of electrically conducting PS/MWCNT/GNP nanocomposites with very high (~20.2 dB) EMI shielding value at extremely low loading of MWCNTs (~2 wt %) and GNP (~1.5 wt %). Finally, through optimizing the ratio of PS–GNP bead and MWCNTs in the nanocomposites, an electrical conductivity of ~9.47 × 10^{-3} S cm^{-1} was achieved at GNP and MWCNTs loading of 0.29 and 0.3 wt %, respectively. The random distribution of the GNPs and MWCNTs with GNP–GNP interconnection through MWCNT in the PS matrix was the key factor in achieving high electrical conductivity and very high EMI shielding value at this low MWCNT and GNP loadings in PS/MWCNT/GNP nanocomposites. With this technique, the formation of continuous conductive network structure of CNT–GNP–CNT and the development of spatial arrangement for strong π–π interaction among the electron rich phenyl rings of PS, GNP, and MWCNT could be possible throughout the matrix phase in the nanocomposites, as evident from the field emission scanning electron microscopy (FESEM) and transmission electron microscopy (TEM) studies.

KEYWORDS: *GNP, MWCNT, EMI, PS bead, electrical conductivity, nanocomposites*

1. INTRODUCTION

Over the last two decades, polymer nanocomposites based on graphite, carbon black, carbon nanofiber, single/multiwall carbon nanotubes (SW/MWCNTs), and graphene have gained enormous interest due to their unique and extraordinary physical and electrical properties and various applications.[1,2] Among these nanofillers, CNT and graphene sheets have been considered to show effective and useful applications in different fields such as sensors,[3] transistors,[4] devices,[5] catalysts,[6] bioluminescent probes,[7] and high-performance[8] and electromagnetic interference (EMI) shielding composites. Although the EMI shielding effectiveness (SE) and electrical properties of the polymer nanocomposites can greatly be enhanced by addition of the CNTs and graphite nanoplates (GNPs) in the polymer matrix, the electrical conductivity of the polymer nanocomposites strongly depends on the ability to homogeneously disperse these nanofillers into the matrix polymer. In conductive polymer nanocomposites, dispersed conductive nanofillers (CNTs or GNP) form a continuous conductive network path in the polymer matrix above a critical concentration of the nanofillers (CNTs/GNP), known as percolation threshold (P_c), which strongly depends on the aspect ratio (length/diameter) of the nanofillers as well as dispersion of the nanofillers into the polymer matrix.

Generally, three different methods, such as (i) in-situ polymerization of monomer in the presence of nanofillers, (ii) solution blending of polymer in the presence of nanofillers, followed by evaporation of solvent, and (iii) melt blending of

Received: December 21, 2012
Accepted: May 2, 2013
Published: May 2, 2013

polymer with nanofillers, are used for the preparation of polymer nanocomposites.

Many researchers[9−13] have reported the EMI shielding properties of various polymer nanocomposites using different nanofillers. For instance, Gupta et al.[9] reported the EMI SE of ∼20 dB for the solution casted PS/MWCNT nanocomposites at 7 wt % loading of MWCNT. Chen et al.[10] reported the EMI SE of ∼21 dB at 15 wt % loading of reduced graphene sheets for the epoxy/reduced graphene based nanocomposites sheets, prepared by solution casting method followed by ultrasonication. Chen et al.[11] reported that the EMI SE of the solution blended polyurethane (PU)/SWCNT nanocomposites was 16−17 dB at 20 wt % loading of SWCNT. Joo et al.[12] reported the EMI SE of ∼27 dB at 40 wt % of MWCNT loading in solution blended PMMA/purified MWCNT nanocomposites. Gupta et al.[13] achieved the EMI SE of ∼19 dB at 15 wt % loading of carbon nanofibers (CNF) in solution casted PS/CNF nanocomposites.

Many groups have been working on PS/CNT nanocomposites prepared by using diverse techniques.[14−25] For instance, Mazinani et al.[14] reported that at 3.5 wt % loading of MWCNT, electrical conductivity of electrospun PS/MWCNT nanocomposites was $\sim 1.02 \times 10^{-5}$ S cm^{-1}, and a considerable increase in electrical conductivity was observed after this concentration. Styrene−butadiene−styrene (SBS) was used as an interfacial agent to improve the dispersion of CNTs in PS solution before electrospinning. Hermant et al.[15] reported that the percolation threshold of PS/SWCNT nanocomposites, prepared by in situ bulk polymerization using conductive poly(3,4-ethylenedioxythiophene) and poly(styrene sulfonate), was 0.3 wt % of SWCNT. Kota et al.[16] reported that solution casted PS/MWCNT nanocomposites showed electrical conductivity ∼1 S.m^{-1} at CNT concentration of 12 vol %. Yang et al.[17] prepared the PS/MWCNT nanocomposites by solution casting method using toluene as a solvent in the presence of nonionic surfactant, polyethylene glycol (PEG). They reported a DC electrical conductivity of $\sim 2.32 \times 10^{-4}$ S m^{-1} at 1 wt % loading of MWCNT in the nanocomposites. Tchoul et al.[18] prepared PS/pulsed laser vaporization (PLV)-SWCNT nanocomposites by solvent evaporation method and reported a DC electrical conductivity of $\sim 10^{-8}$ S cm^{-1} at 1.4 wt % loading of PLV-SWCNT. They also showed the electrical conductivity on the order of 10^{-10} S cm^{-1} at 2 wt % loading of oxidized PLV-SWCNT in PS/oxidized PLV-SWCNT nanocomposites prepared by coagulation method. Grossiord et al.[19] found the percolation threshold in emulsion polymerized PS/SWCNT nanocomposites at 0.3 wt % loading of SWCNT and the electrical conductivity of the nanocomposites was $\sim 10^{-5}$ S cm^{-1} at 2 wt % SWCNT loading. An et al.[20] prepared graphene/MWCNT/PS hybrid nanocomposites by water-based in situ microemulsion polymerization and reported the film resistance of $\sim 2.7 \times 10^{7}$ and $\sim 1.0 \times 10^{5}$ Ω square^{-1} at 2 and 20 wt % MWCNT/graphene mixture in the PS matrix, respectively, indicating that electrical conduction within the composites film occurs via CNT and graphene percolation. Wang et al.[21] reported that the electrical conductivity of suspension polymerized PS/SWCNT nanocomposites was $\sim 4.54 \times 10^{-7}$ S cm^{-1} at 1 wt % SWCNT loading. Zhang et al.[22] prepared PS/MWCNT nanocomposites by in situ bulk polymerization method and reported DC electrical conductivity of $\sim 3.98 \times 10^{-6}$ S cm^{-1} at 5 wt % MWCNT loading. Sun et al.[23] reported the electrical conductivity in solution blended syndiotactic polystyrene (sPS)/MWCNT nanocomposites on the order $\sim 10^{-3}$ S cm^{-1} at 3 wt % of MWCNT loading. Wu et al.[24] reported an electrical conductivity of $\sim 4.9 \times 10^{-4}$ S cm^{-1} at 6.5 wt % MWCNT loading in PS/MWCNT nanocomposites prepared by latex fabrication method. Kara et al.[25] reported the electrical conductivity of the bulk polymerized PS/MWCNT nanocomposites in the order of $\sim 10^{-7}$ S cm^{-1} at 3.5 wt % MWCNT loading.

In the literature, irrespective of the method of polymer/CNT nanocomposites preparation, the working EMI shielding value (∼20 dB) of the nanocomposites was obtained at higher filler loading and also percolation threshold of the CNT in the nanocompoasites in most cases was above 1 wt %. In this study, we have demonstrated a unique and novel method for the preparation of highly EMI shielding and electrically conducting PS/MWCNT/GNP nanocomposites at extremely low CNT and GNP loadings. The method involves in situ bulk polymerization of styrene/MWCNT in the presence of suspension polymerized PS−GNP microbeads. Thus, presence of PS−GNP beads as "excluded volume" and selective localization of the CNTs in the in situ bulk polymerized PS phase increases the effective concentration of the CNTs in the nanocomposites. By optimizing the amount of PS−GNP bead content, PS/MWCNT/GNP nanocomposites with very high (∼20.2 dB) EMI shielding value at extremely low loading of MWCNTs (∼2 wt %) and GNP (∼1.5 wt %) and high electrical conductivity ($\sim 9.47 \times 10^{-3}$ S cm^{-1}) were obtained even at 0.3 wt % MWCNT and 0.29 wt % GNP loadings.

2. EXPERIMENTAL SECTION

2.1. Material Details. Styrene monomer used in this study was of synthesis grade and procured from Merck, Germany. Benzoyl peroxide (BP), used as polymerization initiator, was obtained from Sigma-Aldrich, Inc. MWCNT employed in this study was of industrial grade (NC 7000 series; average diameter of 9.5 nm and length 1.5 μm; surface area 250−300 m^2 g^{-1}; 90% carbon purity), purchased from Nanocyl S.A., Belgium. The MWCNTs were used as received, without any chemical modification. Multilayer graphite nanoplate (GNP, carbon purity >99.5%, thickness 8−10 nm, diameter 5−25 μm, electrical conductivity 10^7 S m^{-1}) was purched from J. K. Impex, Mumbai, India.

2.2. Preparation of the Nanocomposites. *2.2.1. Purification of Styrene Monomer.* Styrene monomer was taken in a 500 mL separating funnel and 25 mL of 5% aq NaOH solution was added into it. The mixture was shaken for 20 min, and the purified styrene was decanted from the aqueous phase in a 250 mL beaker. This process of washing was continued 5 times, and finally, after washing 3 times with deionized water, the purified styrene monomer was collected by passing through anhydrous sodium sulfate (Na_2SO_4).

2.2.2. Suspension Polymerization of Styrene in the Presence of GNP. Purified styrene monomer (25 mL) was taken into 50 mL beaker and calculated amount (0.1 g) of GNP was added into it. The styrene−GNP dispersion was ultrasonicated for 2 h at room temperature and, then, stirred for another 10 min with benzoyl peroxide (BP) (1 wt %) as the polymerization initiator to dissolve the BP in styrene monomer. In a three neck round-bottom (RB) glass reactor fitted with nitrogen (N_2) inlet and refluxing condenser, 600 mL of deionized water was taken and placed in a water bath (connected with the heater) at 80 °C under N_2 atmosphere. Then, polyvinyl alcohol (PVA, 3 wt %) was added into the reactor under constant stirring. After 1 h, the purified styrene−GNP−BP sonicated dispersion was added into the PVA solution in the reactor under constant stirring, in N_2 atmosphere. Then, this mixture was vigorously stirred for 8 h at 80 °C. Finally, after cooling, GNP coated polystyrene (PS) microbeads were filtered and washed with methanol. The PS−GNP beads were first air-dried and, then, kept in an air oven at 60 °C for 12 h.

Scheme 1. Schematic Representation for the Preparation of PS/MWCNT/GNP Nanocomposites

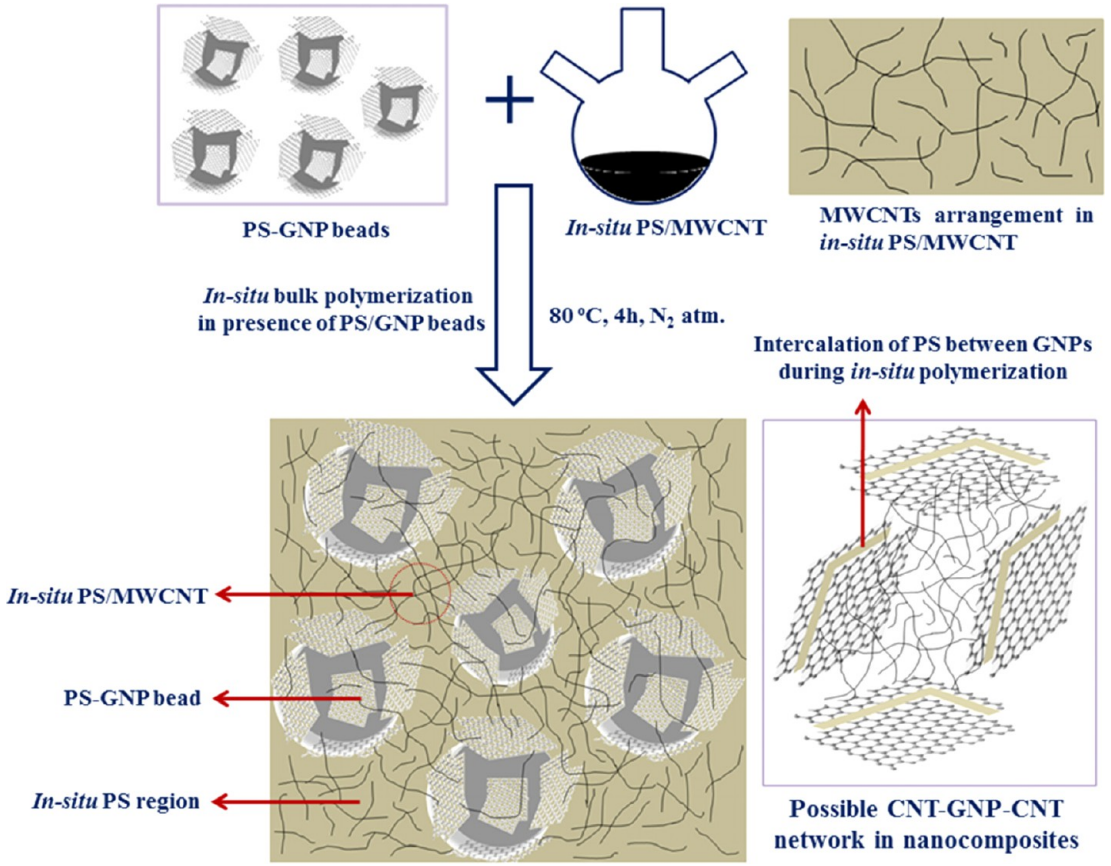

2.2.3. In situ Bulk Polymerization of Styrene/MWCNT in the Presence of PS−GNP Beads. The calculated amount (10 mL) of purified styrene monomer was taken in a 100 mL three-neck reactor and desired amount (0.1 g) of MWCNT was dispersed in the styrene monomer. The styrene−MWCNT dispersion was ultrasonicated for 2 h at room temperature. Then, a refluxing condenser and N_2 inlet were connected at the two necks of the reactor and placed on a magnetic stirrer. BP (1 wt %), as polymerization initiator, was added to the styrene−MWCNT dispersion into the reactor under constant stirring, and the temperature was gradually increased to ∼80 °C. After, 40−50 min of reaction, when the styrene−MWCNT mixture started developing viscosity, 5 g of PS−GNP bead was added into the viscous medium under constant stirring. Addition of the PS−GNP beads into the styrene monomer at the initial stage of polymerization would result in swelling of the PS−GNP beads and, thus, penetration of some CNTs inside the PS−GNP beads. The reaction was continued for 4 h under N_2 atmosphere at constant temperature and stirring. Thus, the PS/MWCNT/GNP nanocomposites were obtained through in situ bulk polymerization of styrene−MWCNTs in the presence of PS−GNP beads. The nanocomposites was first air-dried and finally dried in an air oven at 60 °C for 12 h. From the weight (≈10 g) of the final product, calculated loadings of the MWCNT, GNP, and PS−GNP bead in the PS/MWCNT/GNP hybrid nanocomposites were 0.10, 0.21, and 50 wt %, respectively. The (50/50 w/w) PS-MWCNT/PS−GNP nanocomposites with different MWCNT loadings (0.20, 0.30 wt %) at constant (0.21 wt %) GNP loading, and (50/50 w/w) PS−MWCNT/PS−GNP nanocomposites with 1 wt % MWCNT and 0.65 wt % GNP loadings were also prepared by the same polymerization method. The PS/MWCNT/GNP nanocomposites with higher amount of the PS−GNP bead (60 and 70 wt %) and GNP (0.25, 0.29, 0.65, 0.8, and 1.5 wt %) at various MWCNT loadings (0.1, 0.2, 0.3, 1.5, and 2 wt %) were also prepared through the same polymerization route, by varying the amounts of the styrene monomer, MWCNT, and the PS−GNP bead during the polymerization reaction. Finally, PS/MWCNT/GNP nanocomposites were compression molded at 175 °C in a hot press under constant pressure (8 MPa), and the molded parts were air-cooled to room temperature for further characterizations. The schematic representation for the preparation of the nanocomposites is illustrated in Scheme 1.

2.3. Charaterizations. *2.3.1. Measurement of Electrical Conductivity.* The direct current (DC) conductivity measurements were performed on the compression molded bars of dimensions 30 mm × 10 mm × 3 mm. The sample was cryofractured at two ends, and the fractured surfaces were coated with a thin layer of silver paste to ensure good contact of the sample surface with the electrodes. The DC electrical conductivity of the nanocomposites was measured with a four-probe technique. A minimum of five tests was performed for each specimen, and the average data was reported.

Alternating current (AC) electrical conductivity of the nanocomposites (disc type sample with thickness 0.3 cm and area 1.88 × 10^{-1} cm^2) was obtained using a computer controlled precision impedance analyzer (Agilent 4294A) on application of an alternating electric field across the sample cell in the frequency region of 40 Hz to 10 MHz. The parameters such as dielectric constant (ε') and dielectric loss (ε'') were obtained as a function of the frequency. The AC conductivity (σ_{ac}) was calculated from the dielectric data using the relation:

$$\sigma_{ac} = \omega \varepsilon_0 \varepsilon' \tan \delta \quad (1)$$

Where, $\omega \approx 2\pi f$ (f is the frequency), and ε_0 is the dielectric constant of the vacuum. The dielectric constant (ε') was determined with the following equation:

$$\varepsilon' = C_p/C_0 \quad (2)$$

Where, C_p and C_0 are the capacitance of the sample (in parallel mode) and the cell, respectively. The value of C_0 was calculated using the area (A) and thickness (d) of the sample, following the relation:

$$C_0 = \varepsilon_0 A/d \quad (3)$$

2.3.2. Electromagnetic Interference Shielding Effectiveness (EMI SE). The EMI shielding effectiveness of PS/MWCNT/GNP nanocomposites was measured with a E5071C ENA series network analyzer (Agilent Technologies) using an industrial standard method. Composites slabs of dimensions 25.5 mm × 13 mm × 5.6 mm were measured in the 8.2−12.4 GHz (the so-called X band) frequency range.

2.3.3. I−V Measurement. The current−voltage relationship of PS/MWCNT/GNP nanocomposites was measured with compression molded samples, using a Keithley 2400 source meter (lab view 18.1 protocol). Both sides of the sample were coated with silver paste, and the sample was placed on the probe station, from where two contacts were taken out. Positive voltage was applied from the top contact of the material, using the Keithley source meter.

2.3.4. Fourier Transform Infrared Spectroscopy (FTIR). FTIR of PS and PS/MWCNT/GNP nanocomposites were studied using a NEXUS 870 FTIR (Thermo Nicolet) to investigate the structure of PS and PS/MWCNT/GNP nanocomposite. For the FTIR spectrum, a very thin film of materials was prepared and this film samples were analyzed for getting the spectrum.

2.3.5. Raman Spectroscopy Measurement. Raman spectral of MWCNT, GNP and PS/MWCNT/GNP nanocomposite samples were studied with a Renishaw Raman microscope, equipped with a He−Ne laser excitation source emitting at a wavelength of 632.8 nm and a Peltiercooled (−70 °C) charge-coupled device (CCD) camera. A Leica DMLM microscope was attached and was fitted with three objectives (5×, 20×, 50×). The 20× objective was used for our study. The data acquisition time was 30 s. The slit provided a spectral resolution of 1 cm^{-1}.

2.3.6. Scanning Electron Microscopy (SEM). The morphology of PS−GNP bead was analyzed through SEM instrument (Tescan VEGA-II LSU, Czech Republic). The PS−GNP bead samples were coated with a thin layer of gold (approximately 5 nm) to avoid electrical charging. The vacuum was on the order of 10^{-4} to 10^{-6} mm Hg during scanning, and SEM images were taken from the bead surfaces of the sample.

2.3.7. High Resolution Transmission Electron Microscope (HRTEM). The extent of dispersion of the MWCNTs and GNP in the PS matrix was studied by HRTEM (JEM-2100, JEOL, Japan), operating at an accelerating voltage of 200 kV. The PS/MWCNT/GNP nanocomposites were ultramicrotomed under cryogenic condition with a thickness of around 70−100 nm.

2.3.8. Field Emission Scanning Electron Microscope (FESEM). The surface morphology of the PS−GNP bead and PS/MWCNT/GNP nanocomposites was studied using a Carl Zeiss-SUPRA 40 FESEM, with an accelerating voltage of 5 kV. The molded samples were kept in liquid nitrogen for 20−30 s in a stainless steel container and then broken inside liquid nitrogen. The fractured surfaces of the samples were coated with a thin layer of gold (approximately 5 nm) to avoid electrical charging. The vacuum was on the order of 10^{-4} to 10^{-6} mm Hg during scanning, and FESEM images were taken on the fractured surface of the sample.

3. RESULTS AND DISCUSSION

3.1. Morphology of PS/MWCNT/GNP Nanocomposites. *3.1.1. WAXD Analysis.* Figure 1 shows the X-ray diffractograms of pure PS, GNP powder, PS−GNP beads, and PS/MWCNT/GNP nanocomposites. Pure PS exhibited a wide peak in a broad 2θ region (16.12−24.5°), indicating the amorphous nature of the polymer. For GNP, an intense crystalline peak occurs at a 2θ value of 26.50°, which is the characteristic peak of the hexagonal GNP with a d-spacing of 0.336 nm. It was noteworthy, with the retention of PS peak position (15.96−24.35°), the characteristic peak position ($2\theta \approx$ 26.50°) of the GNP in PS−GNP bead shifted marginally to a lower ($2\theta \approx$ 26.08°) value, indicating a slight increase in the *d*-spacing (0.341 nm) of the GNP layers in the PS−GNP bead.

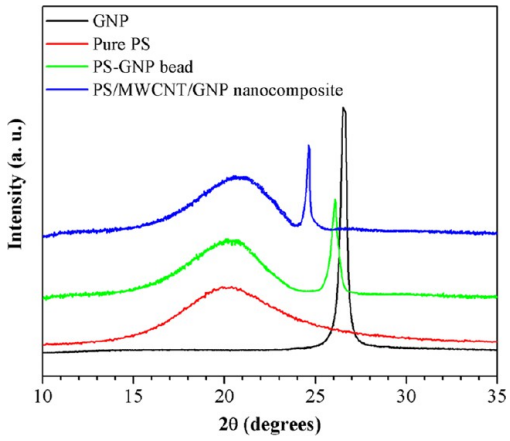

Figure 1. WAXD analysis of pure PS, GNP powder, PS−GNP bead, and PS/MWCNT/GNP nanocomposites. The nanocomposites contains 60 wt % PS−GNP bead with 0.25 wt % GNP and 0.3 wt % MWCNT.

This possibly could be due to the polymerization of minor amount of the styrene monomer inside the GNP layers during the suspension polymerization of styrene in the presence of GNP. In the case of PS/MWCNT/GNP nanocomposites, the characteristic peak for the GNP shifted to a lower region ($2\theta \approx$ 24.46) with a *d*-spacing 0.363 nm. This indicated significant intercalation of the PS chains inside the GNP layers during in situ bulk polymerization of the styrene in the presence of PS−GNP beads. We assume that unreacted styrene monomers effectively penetrated inside the GNP layers during the polymerization although PS−GNP beads were added at a later stage of polymerization. The broad peak for the PS in the PS/MWCNT/GNP composites appeared almost in the same region (16.28−23.95°). However, the presence of a sharp peak for the GNP in the PS−GNP bead and PS/MWCNT/GNP nanocomposites indicated the retention of stacking of hexagonal GNP sheets in the beads as well as in the nanocomposites.

Figure 2 shows the selected area electron diffraction (SAED) pattern images of pure GNP and PS/MWCNT/GNP nanocomposites. The SAED image of pure GNP powder (Figure 2a) indicated the typical 6-fold symmetry and crystalline nature of the GNP powder. However, amorphous behavior is observed in the case of PS/MWCNT/GNP nanocomposites, as shown in part b. This amorphous nature in part b is unambiguously related to the amorphous nature of the PS in the nanocomposites.

3.1.2. FTIR Analysis. Figure 3 shows the FTIR spectrum of the pure PS and PS/MWCNT/GNP nanocomposites. In general, spectral pattern and number of bands for the PS and PS/MWCNT/GNP nanocomposite were more or less similar, apart from their intensity. The peaks for PS and its nanocomposites in the region of 2830−2971, 2986−3093, 1498, and 718−1418 cm^{-1} indicate aliphatic C−H stretching, aromatic C−H stretching, aliphatic $-CH_2$, and different conformation sensitive vibration modes of PS, respectively. The peaks of PS at 2933 and 2854 cm^{-1} were assigned to the asymmetrical and symmetrical stretching vibrations of $-CH_2$, respectively. However, intensity and spectral pattern of these two peaks has slightly been changed in the case of PS/MWCNT/GNP nanocomposites. This might be due to the interaction of PS chains with GNP and MWCNT. The peak at 1455 cm^{-1} was assigned to the flexural vibrations of $-CH_2$. The

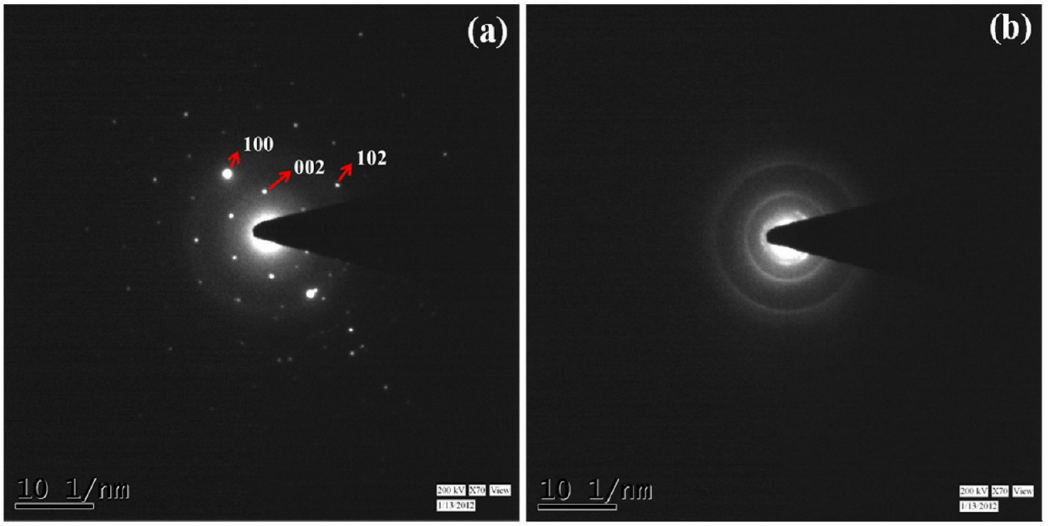

Figure 2. SAED pattern of (a) GNP powder and (b) PS/MWCNT/GNP nanocomposites. The nanocomposites contains 60 wt % PS−GNP bead with 0.25 wt % GNP and 0.3 wt % MWCNT.

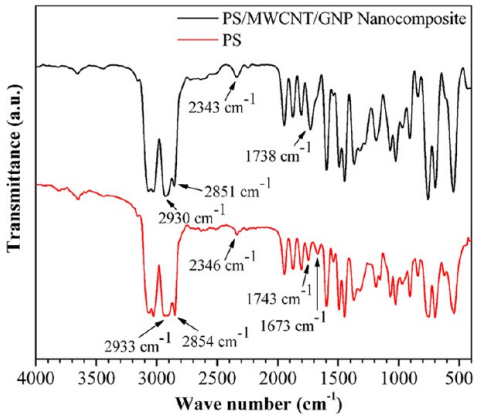

Figure 3. Comparative FTIR analysis of PS and PS/MWCNT/GNP nanocomposites. The nanocomposites contains 60 wt % PS−GNP bead with 0.25 wt % GNP and 0.3 wt % MWCNT.

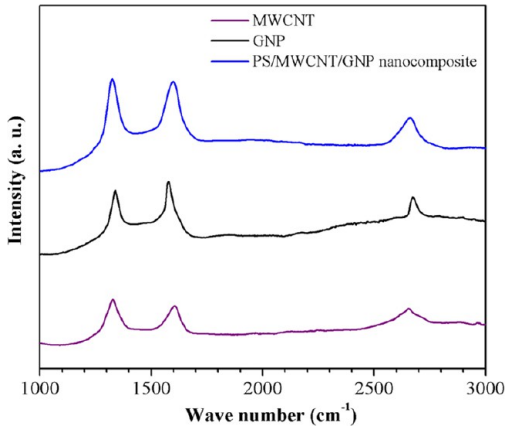

Figure 4. Comparative Raman spectrum analysis of MWCNT, GNP, and PS/MWCNT/GNP nanocomposites. The nanocomposites contains 60 wt % PS−GNP bead with 0.25 wt % GNP and 0.3 wt % MWCNT.

prominent changes in the spectrum were observed in the region of 1637−1779 cm^{-1}. The peaks at 1673 and 1743 cm^{-1} for PS combined to form a new peak at 1738 cm^{-1} in the nanocomposites, which might be due to the formation of a C−C bond between PS with GNP and MWCNT during polymerization initiated by radicals on both the MWCNT and GNP. Moreover, a new peak was appeared at 2343 cm^{-1} in the nanocomposites, which might be due to the interaction between PS and the nanofillers. Many groups[20,26] reported the FTIR of PS/graphene or PS/MWCNT/graphene nanocomposites. The vibrational spectrum of the PS in the region >1500 cm^{-1} consists of a number of absorption bands with little structural characteristics, which indicates that it is extremely difficult to obtain an accurate vibrational assignment and spectroscopic barcode in this region.

3.1.3. Raman Spectroscopy. The Raman spectra of pure MWCNT, GNP, and PS/MWCNT/GNP nanocomposites are shown in Figure 4. This characterization was done with visible (632.8 nm) laser light. From the figure, it is clearly observed that the characteristic peaks for MWCNT appeared at ∼1331 cm^{-1} (1D band) and ∼1604 cm^{-1} (1G band), respectively.

The peak for D band was raised for the breathing modes of sp^2 atoms in the rings and the G peak was developed due to the bond stretching of all pairs of sp^2 atoms in both the rings and chains, which are well-known as the disorder induced and in-plane E_{2g} zone center modes, respectively.[20] In the case of GNP, the G band peak appeared at ∼1576 cm^{-1} along with a peak at 1337 cm^{-1} (1D), and the second-order Raman band spectra (2D) appeared at ∼2683 cm^{-1}. This indicated the absence of a significant number of defects in GNP. However, in the case of PS/MWCNT/GNP nanocomposites, it is clearly seen that the intensity of the D (ID) and G (IG) bands were higher than those of GNP and MWCNT. The 1D/1G ratio for PS/MWCNT/GNP nanocomposites is higher than those of GNP and MWCNT, respectively. This high ratio of the PS/MWCNT/GNP nanocomposites indicates the formation of possible covalent bonds between PS, GNP, and MWCNTs, which partially breaks the sp^2 carbon network and makes a strong interaction among them.

3.1.4. Microscopic Analysis. Figure 5 represents the SEM images of the suspension polymerized PS−GNP beads. As can be seen (Figure 5a), suspension polymerization of styrene monomer/GNP mixture in water medium resulted in the formation of very fine beads with spherical shapes, and the diameter of the beads was in the range of ∼80−110 μm. Figure

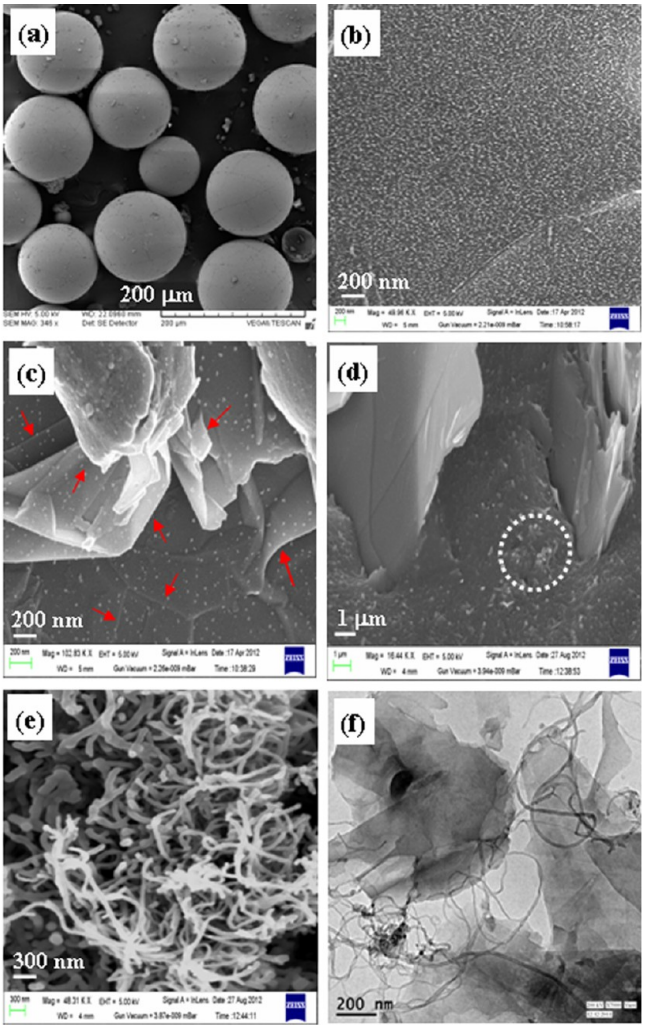

Figure 5. (a) SEM micrograph of PS−GNP beads, (b) field emission SEM micrographs of cross-section area of PS−GNP beads, (c) field emission SEM micrographs of surface of the PS−GNP beads, (d and e) field emission SEM micrographs of PS/MWCNT/GNP nanocomposites at different magnifications, and (f) TEM micrographs of PS/MWCNT/GNP nanocomposites. The nanocomposites contains 60 wt % PS−GNP bead with 0.25 wt % GNP and 0.3 wt % MWCNT.

5b shows the FESEM image of the cross section area of PS−GNP bead. The SEM image of the cross section area (inside the bead) clearly indicated the absence of GNP sheets inside the PS−GNP bead. However, plateletlike GNP sheets were observed on the surface of PS−GNP bead, as shown in higher magnification FESEM image of the beads in Figure 5c. The morphology of the nanocomposites was studied in detail by FESEM and TEM analysis. Figure 5d and e represents the FESEM micrographs of the PS/MWCNT/GNP nanocomposites containing 0.3 wt % MWCNTs and 50 wt % PS−GNP bead. The microstructure (Figure 5d) resembled the presence of CNTs in between the GNP sheets in the PS matrix. We assumed that the CNTs failed to penetrate inside the PS−GNP beads during in-situ polymerization of the styrene−MWCNT in the presence of PS−GNP beads. Thus, CNTs were selectively dispersed in the in-situ polymerized PS regions, outside the PS−GNP beads. This arrangement of the CNTs and PS−GNP beads in the PS matrix of the nanocomposites resulted in the formation of GNP−CNT−GNP network structures throughout the matrix phase. A higher magnification image (Figure 5e) of the selected area in Figure 5d clearly revealed the uniform distribution and individualization of the CNTs in the PS matrix and location of the CNTs in between the platelike GNP sheets in the matrix. From the HRTEM image (Figure 5f), random distribution of high aspect ratio tubelike structures ($d \approx 25-30$ nm) clearly indicated the individualization of the CNTs with retention of their aspect ratio (without much breaking or damage of nanotubes) during composite preparation by melt-mixing. MWCNTs were confined between the GNP sheets and, thus, formed a continuous conductive network structure of GNP−CNT−GNP in the PS matrix. The morphological study led us to conclude that, in PS/MWCNT/GNP nanocomposites, GNPs were randomly distributed in the in-situ polymerized PS matrix, while the CNTs were distributed in between the GNPs that resulted in the formation of GNP−CNT−GNP layer structures in the PS matrix.

3.2. Electromagnetic Interference Shielding Effectiveness (EMI SE). It is believed that the EMI SE of conductive polymer nanocomposites is strongly related to its DC conductivity. The EMI SE of a material is mathematically represented as

$$\text{EMI SE(dB)} = 10\log(P_0/P_t) \quad (4)$$

where P_0 is the incident and P_t is the transmitted or remaining electromagnetic power.

The incident power (P_0) is divided into reflected power (P_r), the absorbed power, and the remaining power (P_t) at the output of the shielding.[27] In general, EMI SE is expressed in decibel (dB) units. For example, an attenuation of the incident beam by a factor of 100 (i.e., 1% transmission) is equivalent to 20 dB (dB) of attenuation.

Figure 6 shows the variation of the EMI shielding effectiveness over the frequency range of 8.2−12.4 GHz (X band) for the nanocomposites with different MWCNT and GNP loadings. It is observed that at a constant frequency region, EMI SE increased with increasing weight percent of MWCNTs and GNP. It is noteworthy that the PS/MWCNT/GNP nanocomposites with 2 wt % MWCNTs and 1.5 wt % GNP loading exhibited the EMI SE value of ~20.2 dB at the X band region, which is to the best of our knowledge the highest EMI SE reported in polymer/MWCNT or polymer/GNP nanocomposites with such a low filler loading. For instance, Ling et al.[28] prepared microcellular polyetherimide (PEI)/graphene foam nanocomposites by solution blending and could achieve an EMI SE value of ~20 dB at 10 wt % graphene loading. Zhang et al.[29] reported EMI SE values in the range of 13−19 dB in solution-blended functionalized poly(methyl methacrylate) (PMMA)/graphene microcellular foam nanocomposites at 5 wt % (1.8 vol %) graphene loading. In another study,[30] they have reported an EMI SE value of ~30 dB at 4.2 vol % graphene with C/O ratio 13.2 (graphene-13.2, prepared by thermal exfoliation of graphene oxide) loading in solution blended PMMA/graphene nanocomposites. This unprecedented shifting of the EMI SE to a higher value (~20.2 dB) at very low MWCNT and GNP content in PS/MWCNT/GNP nanocomposites is attributed mainly to the formation of conducting interconnected network structure of GNP/MWCNT/GNP in the insulating PS matrix. The increase in filler loading increases the number of interconnected GNP−CNT−GNP network structure in the nanocomposites that will interact with the incident radiation and lead to the higher shielding effectiveness. The specific EMI shielding effectiveness

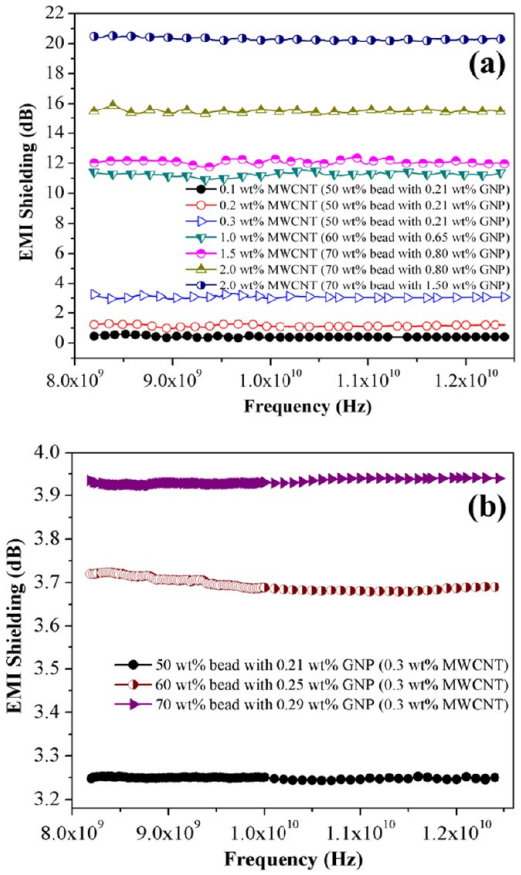

Figure 6. EMI shielding of the PS/MWCNT/GNP nanocomposites vs frequency at (a) different MWCNT loadings with different PS−GNP bead content and (b) various weight percent of PS−GNP beads at constant MWCNT loading (0.3 wt %).

(EMI shielding effectiveness divided by the density) is more appropriate for use in comparing the shielding performance between typical metals and the CNT nanocomposites, particularly in aerospace applications related to EMI shielding. Gupta et al.[9] proposed that the specific EMI SE would be more appropriate when the shielding performance of polymer foams is compared to that of typical metals for aircraft and spacecraft applications. The nanosize of the MWCNT/GNP may provide a larger interfacial area; therefore, the number of conductive interconnected network structures of CNT−GNP increases. Also the high aspect ratio (L/D) of CNTs and GNP helps to create extensively continuous network structures that facilitate electron transport in the nanocomposites with very low fillers loading (2 wt % MWCNT and 1.5 wt % GNP). The target value of the EMI SE needed for commercial applications is around 20 dB (i.e., equal to or less than 1% transmission of the electromagnetic wave). Thus, this investigation indicates that PS/MWCNT/GNP nanocomposites with 2 wt % MWCNT and 1.5 wt % GNP loadings can meet the requirement of commercial applications. When electromagnetic radiation is incident on a slab of material, the absorptivity (A), reflectivity (R), and transmissivity (T) must add up to 1, that is,

$$T + R + A = 1 \tag{5}$$

The absorptivity (A), reflectivity (R), and transmissivity (T) coefficients were obtained by using S parameters, as given below:

$$T = [E_T/E_I]^2 = |S_{12}|^2 = |S_{21}|^2 \tag{6}$$

$$R = [E_R/E_I]^2 = |S_{11}|^2 = |S_{22}|^2 \tag{7}$$

The total EMI SE (SE_{total}) is the sum of the reflection from the material surface (SE_R), the absorption of electromagnetic energy (SE_A), and the multiple internal reflections (SE_M) of electromagnetic radiation, as written below:

$$SE_{total} = SE_A + SE_R + SE_M \tag{8}$$

The reflection is related to the impedance mismatch between air and absorber, the absorption can be regarded as the energy dissipation of the electromagnetic microwave in the absorber, and the multiple reflections are considered as the scattering effect of the in homogeneity within the materials. When $SE_{total} \geq 15$ dB, it is usually assumed that SE_M is negligible and, thus,

$$SE_{total} \approx SE_A + SE_R \tag{9}$$

The effective absorbance (A_{eff}) can be described as[31]

$$A_{eff} = (1 - R - T)/(1 - R) \tag{10}$$

With respect to the power of the effective incident electromagnetic wave inside the shielding material, the reflectance and effective absorbance can be conveniently expressed as[32]

$$SE_R = -10\log(1 - R) \tag{11}$$

$$SE_A = -10\log(1 - A_{eff}) = -10\log[T/(1 - R)] \tag{12}$$

Using the equations given below

$$SE_R = -10\log R \tag{13}$$

$$SE_{total} = -10\log T \tag{14}$$

$$A = 1 - T - R \tag{15}$$

We can therefore get absorptivity (A), reflectivity (R), and transmissivity (T). In this work, for the PS/MWCNT/GNP nanocomposites with 2 wt % MWCNTs and 1.5 wt % GNP loadings, the reflectivity (R), absorptivity (A), and transmissivity (T) are 0.78, 0.215, and 0.005 at 8.2 GHz. Thus, the contribution of reflection to the total EMI SE is much larger than that from absorption. That is, the primary EMI shielding mechanism of such type of nanocomposites is reflection rather than absorption in the X band frequency region. This investigation suggests that the PS/MWCNT/GNP nanocomposites could be considered as a potential composite material for the shielding applications such as construction of lightweight shielding room, etc. Similar results were observed at other frequencies and with other loadings above the percolation threshold.

3.3. Electrical Analysis. *3.3.1. DC Conductivity Measurement.* Figure 7 shows the room temperature DC electrical conductivity (σ_{DC}) of the PS/MWCNT/GNP nanocomposites with different amounts (50, 60, and 70 wt %) of in-situ suspension polymerized PS−GNP bead and MWCNT (0.1, 0.2, and 0.3 wt %) loading. As observed, value of σ_{DC} of the PS/MWCNT/GNP nanocomposites increased with increasing the weight percent of MWCNT, as well as, with increasing weight percent of PS−GNP bead in the nanocomposites. Finally, the PS/MWCNT/GNP nanocomposites with 70 wt % PS−GNP bead and 30 wt % in-situ polymerized PS-MWCNT containing 0.3 wt % loading of MWCNT showed maximum DC electrical conductivity value (~9.47×10^{-3} S cm^{-1}). For instance, the PS/MWCNT composites without any PS−GNP beads did not

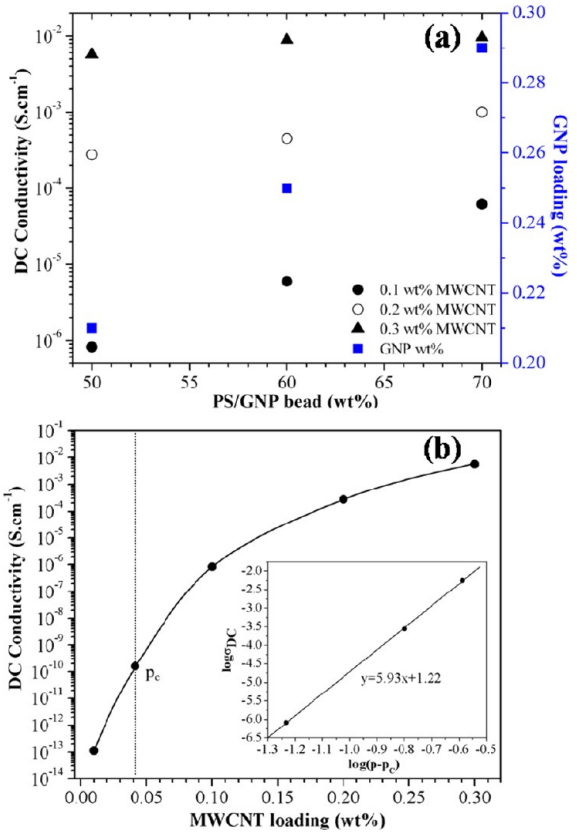

Figure 7. (a) DC conductivity of PS/MWCNT/GNP nanocomposites at different weight percent of PS−GNP beads and GNP loading in the PS matrix with various MWCNT loadings. (b) DC conductivity of PS/MWCNT/GNP nanocomposites with MWCNT loading. (inset) log−log plot of σ_{DC} versus $(p - p_c)$ for the nanocomposites. The straight line in the inset is a least-squares fit to the data using eq 4, giving the best fit values $p_c = 0.041$ and $t = 5.93$.

show any conductivity at 0.1 wt % loading of MWCNT. However, in the case of nanocomposites prepared by in-situ polymerization of styrene−MWCNT in the presence of 50 wt % PS−GNP bead exhibited a DC conductivity of ~8.26×10^{-7} S cm^{-1}. We conclude that the effective concentration of the MWCNT in the in-situ polymerized PS matrix of the nanocomposites increased in the presence of PS−GNP beads and developed a GNP−CNT−GNP continuous conductive network path throughout the PS matrix. The presence of plateletlike GNPs in the PS−GNP beads are also assumed to form a $\pi-\pi$ interaction in between the phenyl ring of PS and GNP sheets and MWCNT after melt blending of the nanocomposites, as schematically shown in Figure 8.

The PS−GNP beads in the matrix can be considered as "excluded volume" into which the sticklike MWCNTs cannot penetrate, and as a result, the concentration of MWCNT has been increased in the region of in-situ polymerized continuous PS phase adjoining the PS−GNP beads. Thus, net σ_{DC} of the nanocomposites was greatly increased due to the presence of PS−GNP beads by developing the GNP−CNT−GNP continuous conductive network path and a $\pi-\pi$ interaction with PS throughout the matrix phase. At the beginning, σ_{DC} of the nanocomposites without any PS−GNP beads at 0.01 wt % of MWCNTs loading was ~1.1×10^{-13} S cm^{-1}, almost similar to the conductivity value of insulating PS matrix. However, σ_{DC} of the nanocomposites drastically increased by several orders (~10^7 order) of magnitude from ~10^{-13} to ~10^{-7} when the nanocomposites was prepared with 0.1 wt % loading of MWCNT in the presence of 50 wt % of PS−GNP bead (containing 0.21 wt % of GNP). This affinity of increase in conductivity undoubtedly indicates the formation of continuous conductive network structure of GNP−CNT−GNP in the nanocomposites, which is well-known as a percolation network. The conductivity of the composites gradually increased on further addition of MWCNT (from 0.1 to 0.3 wt %), as well as, PS−GNP bead (from 50 to 70 wt %) in the PS matrix. Interestingly, the σ_{DC} of the PS/MWCNT/GNP nanocomposites with 70 wt % PS−GNP bead was enormously increased to ~9.47×10^{-3} S cm^{-1} at very low loading (0.3 wt %) of MWCNT. This rapid increase in conductivity of the PS/

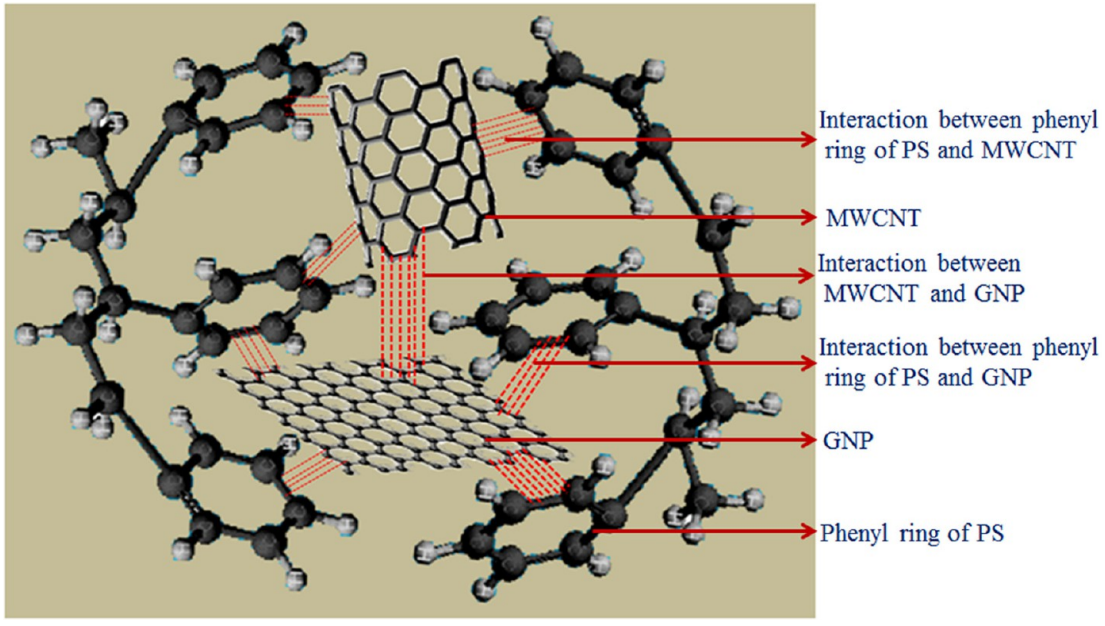

Figure 8. Schematic representation for $\pi-\pi$ interactions between GNP, MWCNT, and PS in the PS/MWCNT/GNP nanocomposites.

MWCNT/GNP nanocomposites at 0.3 wt % of MWCNT loading indicated the development of continuous conductive network structures of the GNP−CNT−GNP in the matrix phase. The percolation theory suggests that the transition from insulator to conductor occurs at a critical concentration (loading) of the conducting filler where the filler particles form a continuous network in the insulating matrix. The minimum concentration (loading) of the conducting filler at which a composites shows a sudden rise in electrical conductivity is known as the percolation threshold (p_c).

The change of DC conductivity with the weight percent (p) of conducting filler in conducting polymer nanocomposites, as shown in Figure 7, was predicted quantitatively on the basis of percolation theory by many researchers.[33,34] The percolation theory has been established by both theoretically and experimentally. Therefore, they discussed the DC conductivity of the polymer nanocomopposites near the percolation threshold (p_c) using power-law behavior:

$$\sigma_{DC}(p) = \sigma_0(p - p_c)^t \qquad \text{for } p > p_c \tag{16}$$

Where, p_c stands for the percolation threshold and t is a critical exponent. The value of the critical exponent depends only on the aspect of the percolation system and independent of the cluster geometry.[8]

The value of t and p_c for the PS/MWCNT/GNP nanocomposites was calculated from the best linear fitted log−log plot of σ_{DC} and $(p - p_c)$ by using eq 16, as shown in the inset of Figure 7b. The calculated value of p_c for the nanocomposites was 0.0415 wt % and the estimated t value was ∼5.93. This linear fit value of PS/MWCNT/GNP nanocomposites by using eq 16 gave an excellent fit with the conductivity of PS/MWCNT/GNP nanocomposites. This result indicated that an extremely low percolation threshold (0.0415 wt % MWCNT loading) was achieved using PS−GNP bead in the PS matrix where plateletlike GNP plays an important role by possible formation of CNT−GNP−CNT network structure and $\pi-\pi$ interaction with phenyl ring of PS matrix (shown in Figure 8) and, thus, enhanced the value of DC electrical conductivity. This very low percolation threshold signifies excellent dispersion and distribution of the high aspect ratio (length/diameter) sticklike MWCNTs and plateletlike GNP in the nanocomposites.

The value $t \sim 5.93$ for the PS/MWCNT/GNP nanocomposites lies very close to the reported value (6.27) for graphite/polyethylene composites,[35] indicating the formation of highly network structure by the GNP and MWCNT in the PS matrix. Many researchers[36,37] have predicted the values of t for two-dimensional (2D) and three-dimensional (3D) lattices from different theoretical calculations. The predicted values for a 2D lattice lie between 1.10 and 1.43, and for a 3D lattice, the predicted values will be lower than 2.02. The real part of the conductivity near the percolation threshold was also predicted to follow a power law.[33]

$$\sigma'(f) \propto f^n \tag{17}$$

The currently accepted values for the critical exponent "n"[38] in 2D ($d = 2$) and 3D ($d = 3$) are ∼0.5 and ∼0.72 for the equivalent circuit model, and ∼0.34 and ∼0.6 for anomalous charge carrier diffusion, respectively. The equivalent circuit model[33,34] assumes a random mixture of capacitors and resistors forming the percolation clusters. In the charge carrier diffusion model,[39] it is assumed that for frequencies $f < f_c$ the charge carriers can explore different clusters within one period, i.e. the diffusion is normal. For frequencies above f_c ($f > f_c$), the charge carriers visit only parts of the percolation cluster within one period and anomalous diffusion at the fractal percolation clusters takes place. This critical frequency f_c also follows a power law:

$$f_c \propto \frac{1}{\tau_\xi} \propto |\varphi - \varphi_c|^{\nu d_w} \tag{18}$$

Where, ν represents the critical exponent related to the cluster size[39] and d_w stands for the effective fractal dimension of the random walk. The correlation time τ_ξ is defined as the time required by the charge carriers to transverse ("explore") a percolation cluster of the correlation length ξ. Balberg et al.[40] showed a relation between the onset of percolation and average excluded volume associated with the nanofillers. If the nanofillers are assumed to be sticks of length L and radius R, and the percolation threshold is expressed as the fractional volume of the nanofiller, p_c, then a relation can be written among these quantities:

$$P_c(L/R) \approx 3 \tag{19}$$

In polymer nanocomposites, conduction occurred by tunneling of charge carriers among nanofillers, this is not only for the physical contact between the nanofillers but also depends on the insulating gaps in their pathways. The effect of tunneling mechanism to the current through the nanocomposites might be one of the reasons for the variations of the conductive properties.[41] The characteristics phenomena of the energy barrier depend on the properties of matrix polymer and also the fabrication process. Trujillo et al.[42] reported that the nanofillers might act as a nucleating agent for semicrystalline polymer on the amount of lamellae that may develop around the CNT.

The electrical conductivity as a result of tunneling conduction has been reported for conducting carbon black (CB) filled various polymer composites. More recently, presence of tunneling conduction has also been reported for CNT composites based on polyvinyl alcohol (PVA) and epoxy resin. Ryvkina et al.[43] proposed a theoretical model for polymer/CB conducting composites where the conduction is dominated by electron tunneling mechanism and expressed the conductivity of a tunnel junction with the relation:

$$\sigma_{DC} \propto \exp(-Ad) \tag{20}$$

Where, A and d represent the tunnel parameter and tunnel distance, respectively.

Several research groups have proposed the conductivity as a result of electron tunneling in various conducting polymer composites, such as, polyepoxy/CNT nanocomposites,[44] polypropylene (PP)/CB composites,[45] and composites. Assuming random or homogeneous distribution of conducting fillers (CB, CNT) in an insulating polymer matrix, it has been proposed that the average distance (tunnel distance, d) among conducting particles in the composites depends on the p value with the relation:

$$d \propto p^{-1/3} \tag{21}$$

It is well-known that the current in a tunnel junction decreases exponentially with the barrier width, which would be here the mean distance among the nanofiller particles. Thus, eq 20 and 21 imply that the value of log σ_{DC} should be

proportional to $p^{-1/3}$. The tunneling assisted conductivity can then be written as

$$\log(\sigma_{DC}) \propto p^{-1/3} \quad (22)$$

As can be seen (Figure 9a), variation of log σ_{DC} for PS/MWCNT/GNP nanocomposites exhibited a linear relationship

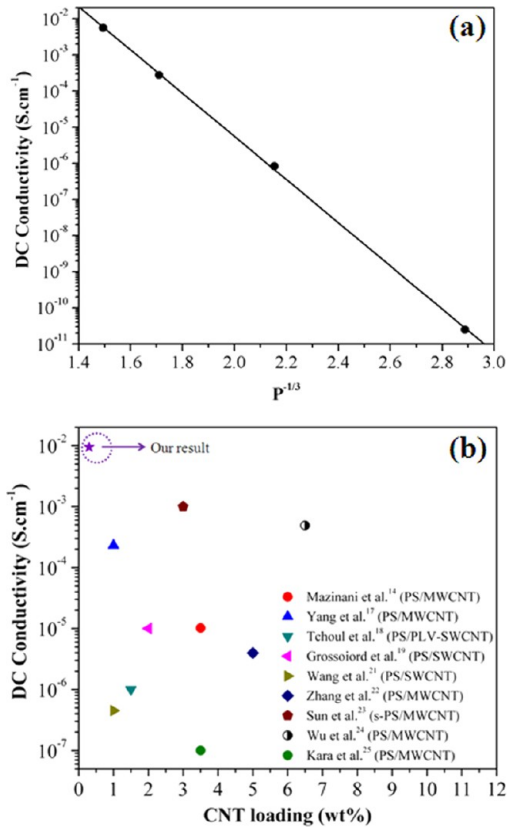

Figure 9. (a) σ_{DC} vs $p^{-1/3}$ for PS/MWCNT nanocomposites. (b) Comparison of our results with different published electrical conductivity data for PS/CNT nanocomposites, prepared by various methods.

with $p^{-1/3}$, indicating the presence of tunneling mechanism behind the electrical conductivity in the nanocomposites. Kilbride et al.[46] reported that coating of individual nanotubes with an insulating polymer led to poor electrical contact between the nanotubes and hence a large contact resistance. When the MWCNTs are separated by a very thin layer of polymer, tunneling of the electrons between the neighboring CNTs occurs through the polymer. This characteristic of conducting current can be attributed to the tunneling of electrons. In general, the electrons in a polymer cannot transfer from one electrode to another through the insulator due to the existence of an energy barrier. However, when a voltage is imposed between the two, the shape of the energy barrier is changed and there is a driving force for the electrons to move across the barrier by tunneling, resulting in a small current when the distance between neighboring electrodes is sufficiently small so that the electrons in the polymer composites are tunneling one by one from one MWCNT electrode to the nearest MWCNT electrode and forming an MWCNT−polymer pathway. It induces resistance and limits the conductivity of the composites. The values reported for the critical exponent in other polymer/CNT systems show a great dispersion.

In the literature,[47] the calculated theoretical critical exponents in three-dimensional (3D) network systems are between 1.6 and 2.0 and experimentally obtained (t) values vary between 1.3 and 3.1. In an experimental study[19] for the solution blended PS/MWCNT composites using dimethyl formamide (DMF) and tetrahydrofuran (THF), the critical exponents were found as 1.5 and 1.9, respectively. Blighe et al. experimentally found the value of $t = 2.2 \pm 0.2$ for PS/SWCNT composites,[48] t = 1.44 for polyepoxy,[44] and much higher t values for HDPE/CB and for HDPE/CNT.[49] The different critical exponents (t) values are related to the microstructural properties (i.e., CNT size, structure, thickness, etc.) of PS/CNT composites.

In the range of CNT loading from 0.01 to 0.3 wt %, the conductivity value of the PS/MWCNT/GNP nanocomposites was drastically increased by several orders of magnitude, from 10^{-13} to 10^{-3} S cm^{-1}. At higher CNT loading between 0.2 and 0.3 wt %, the conductivity stabilized at around 10^{-3} S cm^{-1}, which is the best to our knowledge, the highest value ever reported for PS/MWCNT composites at this low level of CNT loading with unaligned, unmodified, commercially available MWCNTs of similar qualities (carbon purity, aspect ratio). Figure 9b shows the comparative study of the conductivity of the different published data of PS/MWCNT composites. Mazinani et al.[14] reported that, at 3.5 wt % loading of MWCNT, the electrical conductivity of PS/MWCNT nanocomposite was ∼1.02 × 10^{-5} S cm^{-1} and a considerable increase in electrical conductivity is observed after this concentration. Yang et al.[17] reported that the DC electrical conductivity of PS/MWCNT nanocomposite was ∼2.32 × 10^{-4} S m^{-1} with 1 wt % MWCNT loading. Tchoul et al.[18] reported that the DC electrical conductivity of PS/PLV-SWCNT nanocomposite was in the order ∼10^{-8} S cm^{-1} at 1.4 wt % loading of PLV-SWCNT for the poly[(m-phenylenevinylene)-*co*-(2, 5-dioctoxy-*p*-phenylenevinylene)] (PmPV) coated materials. They also showed that the electrical conductivity of PS/oxidized PLV-SWCNT nanocomposites made by coagulation method was in the order of ∼10^{-10} S cm^{-1} at 2 wt % loading of oxidized PLV-SWCNT.

3.3.2. AC Conductivity. As can be seen (Figure 10a), at constant PS−GNP bead content (50 wt %), the AC electrical conductivity of the nanocomposites at constant MWCNT loading increased with the increase in frequency. Furthermore, with the increase in concentration of MWCNT (from 0.1 to 0.3 wt %) at constant PS−GNP bead content, the AC electrical conductivity of the nanocomposites also increased with frequency. This is due to the formation of homogeneous conductive continuous network path throughout the matrix with increasing the concentration of the MWCNT.

From the plot, it is seen that conductivity of the nanocomposites remains almost constant in the frequency region of 50−10^4 Hz and then a rapid increase in the conductivity was prominent in the frequency range of 10^4−10^6 Hz. The frequency independent conductivity, followed by strong dependency, beyond a certain frequency known as critical frequency (f_c).

Figure 10b shows the AC electrical conductivity of the PS/MWCNT/GNP nanocomposites with different PS−GNP bead loading (from 50 to 70 wt %), at constant MWCNT concentration (0.3 wt %) as a function of frequency. It is clearly seen that frequency dependent AC electrical con-

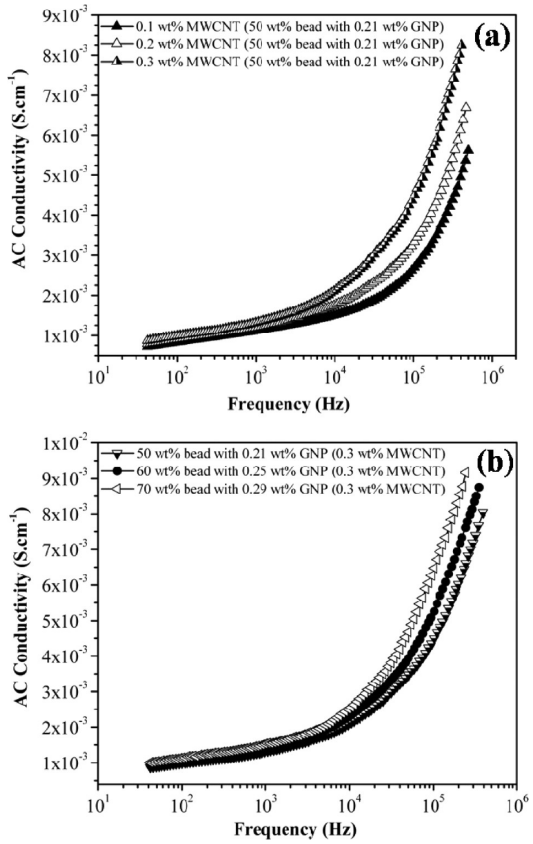

Figure 10. AC conductivity of the PS/MWCNT/GNP nanocomposites vs frequency at (a) different MWCNT loadings at constant PS−GNP beads content and (b) various weight percent of PS−GNP beads at constant MWCNT loading (0.3 wt %).

ductivity of the nanocomposites increased with increasing the PS−GNP bead content at constant MWCNT loading. It can be assume that with increasing the PS−GNP bead content, effective concentration of the MWCNT in PS matrix was increased, since PS−GNP bead acts as excluded volume in the PS phase and rodlike MWCNT can not penetrate inside the bead region. As a result, a uniform continuous conductive network path of GNP−CNT−GNP is formed throughout the PS phase, and thus, effective AC electrical conductivity of the nanocomposites increased with the increasing PS−GNP beads. From the plot, it is clearly seen that conductivity of the nanocomposites remain almost constant up to f_c (in the region of 50−10^4 Hz), and then a sudden increase in the conductivity was observed after f_c in the frequency range of 10^4−10^6 Hz.

Many researchers[50,51] reported that the AC electrical conductivity of the nanocomposites occurred by electron hopping between nanofillers in the PS matrix by an electron tunneling mechanism through the layer structures. The conductivity of the nanocomposites is proportional to the rate of electron hopping and also electron tunneling occurred over a distribution of conductive pathways. The conductive network path of GNP−CNT−GNP or layered structure of CNT/GNP in PS/MWCNT/GNP nanocomposites increases either by increasing MWCNT loading or PS−GNP bead loading, and as a result the rate of electron hopping or tunneling increased. Thus, AC electrical conductivity increased either by increasing MWCNT loading or PS−GNP bead loading in the nanocomposites. The aggregate population of electron tunneling pathways must lie above a percolation threshold of the polymer nanocomposites to get the significant conductivity.

The AC conductivity (σ_{AC}) of any dielectric material at low frequency (below f_c) can be expressed in terms of DC conductivity (σ_{DC}), angular frequency (ω, which is $\approx 2\pi f$), and dielectric loss factor (ε'') with the relation:

$$\sigma_{AC} = \sigma_{DC} + \omega\varepsilon'' \tag{23}$$

The value of σ_{AC} of a dielectric material under frequency is the combination of two components, as shown in eq 23. The first component represents the σ_{DC} which arises from the ionic or electronic conductivity. However, value of the second component ($\omega\varepsilon''$) in the relation depends on the extent of polarization of dipoles (permanent and induced) and accumulated interfacial charges, which is the well-known Maxwell−Wagner−Sillars (MWS) effect. At low frequency (below f_c), the effect of interfacial polarization becomes more significant as the dipoles/induced dipoles get enough time to orient themselves with the direction of applied electric field (relaxation phenomena), and thus, the value of σ_{AC} for a conductive system actually represents the σ_{DC}. The frequency independent electrical conductivity up to a certain frequency (f_c) has already been reported for several disordered materials.[42,46]

At high frequency (above f_c), the polarization effect becomes insignificant as the dipoles get less relaxation time to orient themselves in the direction of applied electric field. The applied AC electric field (periodic alternation) above f_c results in the radical reduction of space charge accumulation and dispersion of dipoles in the applied field direction which decrease in proportion to polarization. Thus, the value of σ_{AC} strongly depends on the excitation of the charge particles and flow of electrons through the continuous conductive network in the matrix phase. Furthermore, it can be assumed that above f_c, the hopping of excited electrons through the inter particle gap (thin polymer layer) becomes easier; adding to the conductivity that already exists at low frequency in the composites.

3.4. *I*−*V* Measurement. Figure 11 shows the current (I)−voltage (V) relationship of the PS/MWCNT/GNP nanocomposites.

As can be seen, at low voltage, current increased with increasing the applied voltage up to 0.8 V, and after this voltage (0.8 V), current become saturated with the voltage for the PS/MWCNT/GNP nanocomposites. We assumed that in the low voltage region (0−0.8 V), thermal excitation energy (KT) (<KT = 25 meV) of the nanocomposites is very low. Hence, generation of the phonons in the nanocomposites is insignificant; therefore, electrons moved freely in the nanocomposites without any scattering with phonons. However, current become saturated beyond the applying voltage of 0.8 V for PS/MWCNT/GNP system. At high voltage, thermal excitation energy of the nanocomposites is very high (≫KT), and a huge amount of phonon has been generated in the nanocomposites. This leads to scattering of electrons by the phonons during movement in the nanocomposites which increases the resistance of the nanocomposites. Thus, electrons are strongly scattered with optical and zone-boundary phonons, and thermal excitation energy becomes very high. At large voltages, the increased energy of charge carriers is sufficient for emission of optical or zone-boundary phonons which cause saturation of the current.

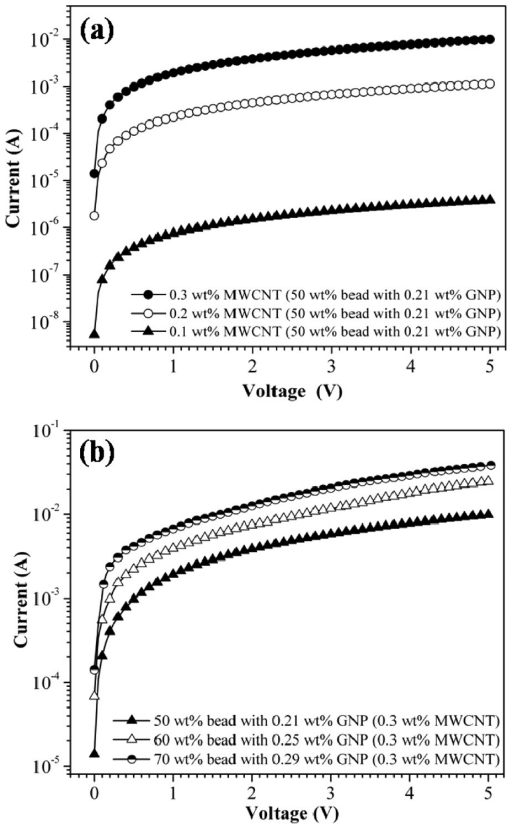

Figure 11. Current (I)−voltage (V) characteristic of the PS/MWCNT/GNP nanocomposites at (a) different MWCNT loadings at constant PS−GNP beads content and (b) various weight percent of GNP beads at constant MWCNT loading (0.3 wt %).

4. CONCLUSION

We have demonstrated a unique method for the preparation of highly conductive PS/MWCNT/GNP nanocomposites with very high EMI value by using PS−GNP beads during polymerization of styrene/MWCNT. The commercially applicable EMI SE value (~20.2 dB) of the PS/MWCNT/GNP nanocomposites has been achieved at very low filler concentration (2 wt % loading of MWCNT and 1.5 wt % loading of GNP), and hence, the PS/MWCNT/GNP nanocomposites can be used in different fields of application such as lightweight shielding rooms, mobile cell phones, spacecraft, aerospace, etc. By optimizing the ratio of PS−GNP bead and MWCNT in the nanocomposites, an electrical conductivity of ~9.47×10^{-3} S cm^{-1} was achieved at extremely low MWCNT loading (0.3 wt %) and 0.29 wt % GNP loading, which has not ever been reported. Here, plateletlike GNP played an important role to increase the EMI SE property as well as electrical conductivity of the nanocomposites. The GNP sheets make strong physical bonds with the PS by $\pi-\pi$ interaction and form a GNP−CNT−GNP interconnected conductive network structure throughout the matrix that reduced the percolation threshold of the nanocomposites. FESEM and HRTEM images indicated the possible formation of GNP−CNT−GNP network structure in the nanocomposites.

AUTHOR INFORMATION

Corresponding Author

*E-mail address: khatuabb@matsc.iitkgp.ernet.in. Tel.: +91 3222 283982. Fax: +91 3222 255303.

Notes

The authors declare no competing financial interest.

ACKNOWLEDGMENTS

We thank the Council of Scientific and Industrial Research (CSIR), New Delhi, India, for financial support.

REFERENCES

(1) Moniruzzaman, M.; Winey, K. I. *Macromolecules* **2006**, *39*, 5194−5205.
(2) Vigolo, B.; Penicaud, A.; Coulon, C.; Sauder, C.; Pailler, R.; Journet, C.; Bernier, P.; Poulin, P. *Science* **2000**, *290*, 1331−1334.
(3) Chiu, H.-Y.; Hung, P.; Postma, H. W. C.; Bockrath, M. *Nano Lett.* **2008**, *8*, 4342−4346.
(4) Xiao, K.; Liu, Y.; Hu, P.; Yu, G.; Sun, Y.; Zhu, D. *J. Am. Chem. Soc.* **2005**, *127*, 8614−8617.
(5) Vijayaraghavan, A.; Blatt, S.; Weissenberger, D.; Carl, M. O.; Hennrich, F.; Gerthsen, D.; Hahn, H.; Krupke, R. *Nano Lett.* **2007**, *7*, 1556−1560.
(6) Tang, Y.; Allen, B. L.; Kauffman, D. R.; Star, A. *J. Am. Chem. Soc.* **2009**, *131*, 13200−13201.
(7) Yang, R.; Jin, J.; Chen, Y.; Shao, N.; Kang, H.; Xiao, Z.; Tang, Z.; Wu, Y.; Zhu, Z.; Tan, W. *J. Am. Chem. Soc.* **2008**, *130*, 8351−8358.
(8) Ci, L.; Suhr, J.; Pushparaj, V.; Zhang, X.; Ajayan, P. M. *Nano Lett.* **2008**, *8*, 2762−2766.
(9) Yang, Y.; Dudley, K. L.; Lawrence, R. W.; Gupta, M. C. *Nano Lett.* **2005**, *5*, 2131−2134.
(10) Liang, J.; Wang, Y.; Huang, Y.; Ma, Y.; Liu, Z.; Cai, J.; Zhang, C.; Gao, H.; Chen, Y. *Carbon* **2009**, *47*, 922−925.
(11) Liu, Z.; Bai, G.; Huang, Y.; Ma, Y.; Du, F.; Li, F.; Guo, T.; Chen, Y. *Carbon* **2007**, *45*, 821−827.
(12) Joo, J.; Kim, H. M.; Kim, K.; Lee, C. Y.; Cho, S. J.; Yoon, H. S.; Pejakovic, D. A.; Yoo, J. W.; Epstein, A. J. *Appl. Phys. Lett.* **2004**, *84*, 589−591.
(13) Gupta, M. C.; Yang, Y.; Dudley, K. L.; Lawrence, R. W. *Adv. Mater.* **2005**, *17*, 1999−2003.
(14) Mazinani, S.; Ajji, A.; Dubois, C. *Polymer* **2009**, *50*, 3329−3342.
(15) Hermant, M.-C.; Schoot, P. V.; Klumperman, B.; Koning, C. E. *ACS Nano* **2010**, *4*, 2242−2248.
(16) Kota, A. K.; Cipriano, B. H.; Duesterberg, M. K.; Gershon, A. L.; Powell, D.; Srinivasa, R. R.; Bruck, H. A. *Macromolecules* **2007**, *20*, 7400−7406.
(17) Yang, Y.; Gupta, M. C.; Zalameda, J. N.; Winfree, W. P. *Micro Nano Lett.* **2008**, *3*, 35−40.
(18) Tchoul, M. N.; Ford, W. T.; Ha, M. L. P.; Chavez-Sumarriva, I.; Grady, B. P.; Lolli, G.; Resasco, D. E.; Arepalli, S. *Chem. Mater.* **2008**, *20*, 3120−3126.
(19) Grossiord, N.; Miltner, H. E.; Loos, J.; Meuldijk, J.; Mele, B. V.; Koning, C. E. *Chem. Mater.* **2007**, *19*, 3787−3792.
(20) An, J.-H.; Patole, A. S.; Patole, P. S.; Jung, S.-Y.; Yoo, J.-B.; Kim, T.-H. *Eur. Polym. J.* **2012**, *48*, 252−259.
(21) Wang, Z.; Lu, M.; Li, H.-L.; Guo, X.-Y. *Mater. Chem. Phys.* **2006**, *100*, 77−81.
(22) Zhang, B.; Fu, R. W.; Zhang, M. Q.; Dong, X. M.; Lan, P. L.; Qiu, J. S. *Sens. Actuators B* **2005**, *109*, 323−328.
(23) Sun, G.; Chen, G.; Liu, Z.; Chen, M. *Carbon* **2010**, *48*, 1434−1440.
(24) Wu, T.-M.; Chen, E.-C. *Compos. Sci. Technol.* **2008**, *68*, 2254−2259.
(25) Kara, S.; Arda, E.; Dolastir, F.; Pekcan, O. *J. Colloid Interface Sci.* **2010**, *344*, 395−401.
(26) Patole, A. S.; Patole, S. P.; Kang, H.; Hoo, J.-B.; Kim, T.-H.; Ahn, J.-H. *J. Colloid Interface Sci.* **2010**, *350*, 530−537.
(27) Thomassin, J.-M.; Lou, X.; Pagnoulle, C.; Saib, A.; Bednarz, L.; Huynen, I.; Jerome, R.; Detrembleur, C. *J. Phys. Chem. C* **2007**, *111*, 11186−11192.
(28) Ling, J.; Zhai, W.; Feng, W.; Shen, B.; Zhang, J.; Zheng, W. *ACS Appl. Mater. Interfaces.* **2013**, *5*, 2677−2684.

(29) Zhang, H.-B.; Yan, Q.; Zheng, W.-G.; He, Z.; Yu, Z.-Z. *ACS Appl. Mater. Interfaces* **2011**, *3*, 918−924.
(30) Zhang, H.-B.; Zheng, W.-G.; Yan, Q.; Jiang, Z.-G.; Yu, Z.-Z. *Carbon* **2012**, *50*, 5117−5125.
(31) Li, N.; Huang, Y.; Du, F.; He, X.; Lin, X.; Gao, H.; Ma, Y.; Li, F.; Chen, Y. S.; Eklund, P. C. *Nano Lett.* **2006**, *6*, 1141−1145.
(32) Wang, J.; Xiang, C.; Liu, Q.; Pan, Y.; Guo, J. *Adv. Funct. Mater.* **2008**, *18*, 2995−3002.
(33) Bergman, D. J.; Imry, Y. *Phys. Rev. Lett.* **1977**, *39*, 1222−1225.
(34) Stephen, M. J. *Phys. Rev. B* **1978**, *17*, 4444−4453.
(35) Ezquerra, T. A.; Kulescza, M.; Santa-Cruz, C.; Balta-Calleja, F. J. *Adv. Mater.* **1990**, *2*, 597−600.
(36) Fisch, R.; Harris, A. B. *Phys. Rev. B* **1978**, *18*, 416−420.
(37) Gingold, D. B.; Lobb, C. J. *Phys. Rev. B* **1990**, *42*, 8220−8224.
(38) Stauffer, D.; Aharony, A. *Introduction to percolation theory*; Taylor & Francis Ltd, London, 1994.
(39) Gefen, Y.; Aharony, A.; Alexander, S. *Phys. Rev. Lett.* **1983**, *50*, 77−80.
(40) Balberg, I.; Binenbaum, N.; Wagner, N. *Phys. Rev. Lett.* **1984**, *52*, 1465−1468.
(41) Grossiord, N.; Loos, J.; van Laake, L.; Maugey, M.; Zakri, C.; Koning, C. E.; Hart, A. J. *Adv. Funct. Mater.* **2008**, *18*, 3226−3234.
(42) Trujillo, M.; Arnal, M. L.; Muller, A. J.; Laredo, E.; Bredeau, S.; Bonduel, B.; Dubois, P. *Macromolecules* **2007**, *40*, 6268−6276.
(43) Ryvkina, N.; Tchmutin, I.; Vilcakova, J.; Peliskova, M.; Saha, P. *Synth. Met.* **2005**, *148*, 141−146.
(44) Barrau, S.; Demont, P.; Peigney, A.; Laurent, C.; Lacabanne, C. *Macromolecules* **2003**, *36*, 5187−5194.
(45) Petrovic, Z. S.; Martinovic, B.; Divjakovic, V.; Budinski-Simendic, J. *J. Appl. Polym. Sci.* **1993**, *49*, 1659−1669.
(46) Kilbride, B. E.; Coleman, J. N.; Fraysse, J.; Fournet, P.; Cadek, M.; Drury, A.; Hutzler, S.; Roth, S.; Blau, W. J. *J. Appl. Phys.* **2002**, *92*, 4024−4030.
(47) Weber, M.; Kamal, M. R. *Polym. Compos.* **1997**, *18*, 711−725.
(48) Blighe, F. M.; Hernandez, Y. R.; Blau, W. J.; Coleman, J. N. *Adv. Mater.* **2007**, *19*, 4443−4447.
(49) Linares, A.; Canalda, J. C.; Cagiao, M. E.; Garcia-Gutierrez, M. C.; Nogales, A.; Martin-Gullon, I.; Vera, J.; Ezquerra, T. A. *Macromolecules* **2008**, *41*, 7090−7097.
(50) Dickinson, E.; Masui, H.; Williams, M. E.; Murray, R. W. *J. Phys. Chem. B* **1999**, *103*, 11028−11035.
(51) Terrill, R. H.; Postlethwaite, T. A.; Chen, C.-H.; Poon, C.-D.; Terzis, A.; Chen, A.; Hutchison, J. E.; Clark, M. R.; Wignall, G.; Londono, J. D.; Superfine, R.; Falvo, M.; Johnson, C. S., Jr.; Samulski, E. T.; Murray, R. W. *J. Am. Chem. Soc.* **1995**, *117*, 12537−12548.